RevMexAA (Serie de Conferencias), **28**, 93–102 (2007)

THE HUBBLE-DEPTH SURVEY

Changbom Park[1] and Juhan Kim[1]

RESUMEN

Mediante una simulación de N cuerpos de un modelo ΛCDM hemos desarrollado una búsqueda de galaxias ficticias hasta la profundidad del Hubble. Para encontrar las galaxias en la distribución de partículas, identificamos los halos estables y autoligados mediante un método de búsqueda de halos en el espacio real y en el cono de luz. Suponemos que cada halo contiene solamente una galaxia con un brillo monotónicamente proporcional a la masa del halo, para así ajustar la función de masa con la función de luminosidad galáctica obtenida en el Sloan Digital Sky Survey (SDSS). Después de aplicar la correcciones K, y de evolución a las luminosidades observadas de las galaxias ficticias, hicimos estudios del corrimiento al rojo bajo varias restricciones observacionales. En particular, proponemos un nuevo estudio de corrimientos al rojo, llamado el Hubble Depth Survey, el cual está limitado hasta la magnitud $r^* = 22$ y alcanza la distancia de Hubble $d_H = 3000\ h^{-1}$ Mpc.

ABSTRACT

We have made a mock galaxy survey of the Hubble depth in an N-body simulation of the ΛCDM model. To populate galaxies in the particle distribution, we identify self-bound and stable halos by a halo finding method in the real and lightcone space. We assume that each halo contains only one galaxy with brightness monotonically proportional to the halo mass to match the mass function with the galaxy luminosity function obtained in the Sloan Digital Sky Survey (SDSS). After applying the $K-$ and evolutionary corrections to the observed luminosity of the mock galaxies, we have made mock redshift surveys under various observational constraints. In particular, we propose a new redshift survey, named the Hubble Depth Survey, which is magnitude-limited down to $r^* = 22$ and reaching the Hubble distance, $d_H = 3000\ h^{-1}$ Mpc.

Key Words: **SURVEYS — METHODS: N-BODY SIMULATIONS — COSMOLOGY**

1. INTRODUCTION

The last two decades have seen an immense expansion of our knowledge of the universe due to a series of large redshift surveys. After obtaining the first-light image in 1998, the Sloan Digital Sky Survey (York et al. 2000; Stoughton et al. 2002; Abazajian et al. 2003) has been observing galaxies, quasars, and other targets while stacking up the photometric and spectroscopic data. Prior to this, there had been several projects: the Las Campanas Redshift Survey (Shectman et al. 1996), Two-degree Field Galaxy Redshift Survey (Colless 1999), CfA (Huchra et al. 1988), Stromlo-APM (Loveday et al. 1992), Durham/UKST Galaxy Redshift survey (Ratcliff et al. 1998), and ESO Slice Project Galaxy Redshift Survey (Zucca et al. 1997), providing the cornerstone data for the study of the large-scale structure (LSS) of the universe. These redshift survey data have been used to measure statistics such as the power spectrum (Park et al. 1994), the correlation function (Park & Lee 1998), topology of the galaxy number density field (Park & Choi 2005), and the power spectrum of the peculiar velocity field (Park & Park 2006). These statistics are used to constrain various cosmological parameters as well as galaxy formation mechanisms.

Prompted by the great success of the SDSS, many next-generation redshift surveys are planned. Most of these surveys intend to observe the era of galaxy and quasar formation in a sufficient volume. There are two kinds of galaxy surveys. One adopts redshifts derived from the photometric observation of galaxies. The other additionally uses spectroscopic information. The advantage of photometric redshift surveys is that the survey volume is bigger and the sample is closer to the fair sample relative to the spectroscopic survey at a given cost and time. The photometric redshifts are useful when one is interested in physics at very large scales and is equipped with very good understanding of the K- and evolutionary corrections. The spectroscopic observation of galaxies is indispensable for precision cosmology and for constraining models of galaxy formation and evolution.

[1]Korea Institute for Advanced Study, 207-43, Cheongnyangni 2-dong, Dongdaemun-gu, Seoul, 130-722, Korea (cbp@kias.re.kr).

TABLE 1

CHARACTERISTICS OF PLANNED FUTURE SURVEYS

Project	$D(m)$[a]	R_{max}	N_{tot}	$\Sigma(\deg^{-2})$[b]	$\Delta\Omega(\deg^{-2})$[c]	Δt (hours/nights)	Starting year
KAOS (low–z)	8.1	22.7	2×10^6	1000	2000	1530/153	2012
KAOS (high–z;FMOS[d])	8.1	24.5	6×10^5	2000	300	1360/136	2012
Pan-STARS (Median Deep)	1.8×4	27.0	2×10^{10}	16000000	1200	40/4	(?)
Pan-STARS (Ultra Deep)	1.8×4	29.0	2×10^{10}	?	28	40/4	(?)
LSST	8.4	26.5	3.6×10^{10}	1800000	20000–30000	a few days	2012

[a]Aperture size of telescope.
[b]Mean surface density.
[c]Survey solid angle.
[d]A joint project between UK and Japan with the Subaru telescope; http://www.aao.gov.au/AAO/local/www/rgs/work/stuff/FUWS-proposal-Jan06v2.pdf

There are several future redshift survey projects currently proposed. The KAOS (kilo-aperture Optical Spectrograph) project[2] is to characterize the properties of dark matter and to investigate the formation and evolution of galaxies and quasars by the WFMOS (Wide-Field Fiber-Fed Optical Multi-Object Spectrograph) instrument that will be mounted on an 8-m class telescope (either the Gemini or the Subaru telescopes). More than two million galaxies and quasars over 2000 deg^2 are planned to be observed for 170 days. But the target sampling is *sparse* since the interest lies only in the geometrical effect of cosmological parameters on the very large-scale galaxy distributions. Pan-STARS, a photometric survey, will be dedicated to short-exposure observations of nearby targets such as solar system objects and variable stars as well as extra galactic sources. It will use four 1.8 meter diameter telescopes. Two sub-projects are proposed to cover three quarters of the entire sky with $r_{lim} = 25.6$ and 1200 deg^2 with $r_{lim} = 27$ (or 29). Another project to cover a large fraction of the whole sky by photometric observations is the LSST[3]. Table 1 lists the characteristics of several future survey projects.

2. HUBBLE DEPTH SURVEY

Since spectral lines of galaxies are typically used to measure galactic redshifts, it is impossible to get reliable redshift information if there is no observable spectral line in the background continuum. There are no obvious emission or absorption lines between Lyα ($\lambda = 1216$Å) and O II (3227Å) in galaxy spectra and, therefore, it is hard to spectroscopically observe galaxies in $1.3 \lesssim z \lesssim 2.5$ in optical bands; hence, this region is often named the *redshift desert.* Because more distant galaxies become fainter by a factor of $1/(1+z)^4$ (due to the cosmological surface dimming effect), it is difficult to get clear spectral lines of galaxies beyond $z = 2.5$ with reasonable cost of telescope resources. Consequently, shallow optical observations of galaxies are both spectroscopically and photometrically limited to $z \lesssim 1.4$ (10 billion years after the Big Bang) which corresponds to the Hubble distance $d_H = 3000\ h^{-1}$ Mpc in the co-moving length. Also, this characteristic distance or epoch is essential to the study of formation and evolution of galaxies and quasars since the star formation rate is believed to peak at $z \lesssim 1$ (Hogg 2002; Madau et al. 1996; *cf.* Baldry et al. 2002).

We propose a Hubble depth survey (HDS) out to a distance of $d_H = 3000\ h^{-1}$ Mpc, the Hubble distance, from which we can generate a volume-limited sample of galaxies with $\mathcal{M}_r \leq -21 + 5\log_{10} h$. The faint limit is roughly the characteristic magnitude, $\mathcal{M}_r^*$ (Blanton et al. 2001). Hereafter, the Hubble constant term in the absolute magnitude is omitted for brevity, otherwise it will be explicitly stated.

2.1. *Required System Characteristics*

We have determined the main characteristics of the HDS to meet the survey purpose specified above. The baseline of the observational instrument for the HDS as follows: the aperture size of the telescope should be at least 6.5-m allowing simultaneous spectroscopic observation of 5000 sources by fibers with a medium resolution of $\mathcal{R} = 2000$ covering 0.4 – 1 μm. The field-of-view should be ~ 1 degree in diameter. For the cosmological study, we want to obtain a volume-limited sample of galaxies of $\mathcal{M}_{r^*} < -21$ to the distance, $z \simeq 1.4$, and the corresponding integrated target surface density is predicted to be $17000\,\deg^{-2}$ (for derivation, see § 3). Table 2 lists several characteristic values of the HDS. Here, the

[2]http://www.noao.edu/kaos/
[3]Large Synoptic Survey Telescope, http://www.lsst.org/

TABLE 2

CHARACTERISTICS OF THE HDS

quantity	value	description
D	6.5	aperture size of telescope in *meter*
R_{max}	22	faint limit of apparent magnitude
Σ	17000	mean surface density of galaxies (deg^{-2})
$\Delta\Omega$	295	survey solid angle (deg^2)
N	5×10^6	total sample number
N_{fiber}	5000	number of fibers on the focal plane
$\mathcal{R}$	2000	spectral resolution
Δt	6000	observational time in hours

exposure time of the spectroscopic observation is roughly calculated to be 6 hours by an extrapolation of the case of the SDSS spectroscopic observations, and the derivation of the mean surface density of galaxies will be provided in § 3.

3. MOCK SURVEY OF THE HDS

3.1. *N-body Simulation*

To model the HDS we have performed 1024^3 particle simulations in a cubic volume of a side length 1024 h^{-1} Mpc from $z = 23$ to $z = 0$, evolved by the GOTPM code (Dubinski et al. 2004). The cosmological parameters adopted are $\Omega_m = 0.27$, $\Omega_b = 0.046$, $\Omega_\Lambda = 0.73$, $h = 0.71$, and $\sigma_8 = 0.9$ which were chosen to reconcile observations of the large-scale structure with the cosmic microwave background anisotropy (see Spergel et al. (2003) for the results from the WMAP experiment). Four mock observers are located at (0,512,η) h^{-1} Mpc looking in the direction of (1,0,0.25) and two replicas of the simulation box are periodically laid in the x direction to reach a maximum observational depth of $z_{max} = 1.5$. The value of η for each observer is 0, 256, 512, and 768, respectively. At each time step, particle data in the lightcone shell are stacked. Since a particle may traverse the *isotime* boundary surface between two consecutive simulation steps, we save particles in the upper and lower buffer shells around the local lightcone region. The width of the buffer shell is set to be the maximum displacement of particles (~ 0.1 times the mean particle separation) at a step. If a particle exists in two neighboring lightcone regions or buffer shells, the positions and velocities of the particle are averaged.

3.2. *Halo Finding*

We apply the Physically Self-Bound (PSB) method (Kim & Park 2006) to extract virialized and self-bound halos. This method has proved to outrange other methods such as the HOP and DENMAX in that the identified sub-halos are tidally stable and the background host halo has no obvious substructure. Moreover, the canonical parameters of the PSB do not show any dependence on the local environments. On the other hand, the halo distributions found by the HOP and DENMAX might differ with different parameter sets and one has to modify the parameter values according to the size of structures of interest.

We apply the PSB method to the snap-shot particle data at several redshifts. But halo identification in the lightcone space needs a modification of the original code since the time in each position of lightcone space is different. We apply this varying-epoch scheme only to particle groups and halos but not to individual particles to reduce the computational overhead. The cosmological time of each group is measured with respect to its center of mass.

4. OBSERVATIONAL RESOURCES

To make mock survey in a given cosmology one needs to construct a distribution of galaxies in space, and one needs to know the number density of galaxies as a function of redshifts. For this purpose we use the number density of dark matter halos obtained by Kim & Park (2006), who derived halo mass functions using a 2048^3 particle simulation in the concordance LCDM model. We distinguish two definitions of halos: one is the FoF halo that is a group of chained particles, and the other is the physically self-bound (PSB) halo whose particle members are gravitationally bound to a local center and confined within the tidal radius (Kim & Park 2006). A small PSB halo may be hosted by other larger PSB halos but considered as a separate halo while, by definition, a FoF halo may not. Sub-halos in an FoF group are regarded as substructures. Secondly, galaxies are assigned to halos under simple assumptions. We apply the one-to-one correspondence model (*cf.* Neyrink et al. 2004) between a PSB halo and a galaxy. In other words, every halo above a certain mass threshold is supposed to have one and only one galaxy. And, moreover, the luminosity of the mock galaxy is assumed to be a monotonic function of the host halo mass. The detailed model descriptions will be provided in §3.

4.1. *Halo Distributions in the Real Space*

In Figure 1 we show halo mass functions in real space at various redshifts. Our halo mass functions

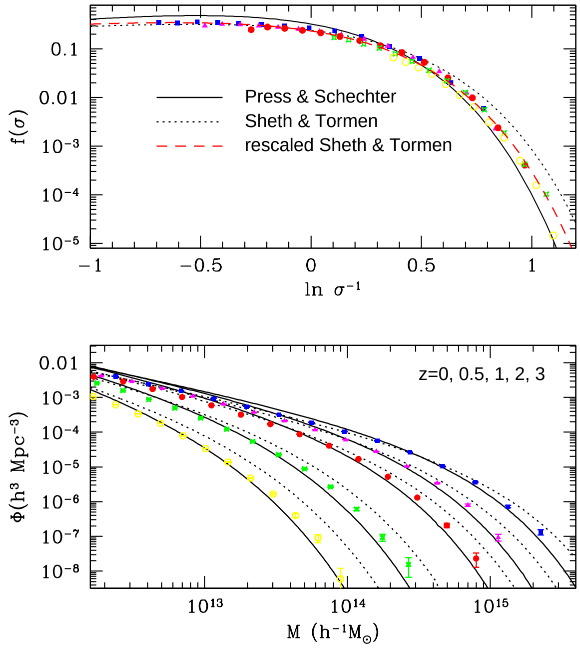

Fig. 1. Mass function of halos. *Lower panel*: Halo mass functions obtained at various redshifts are plotted with two analytic functions, the Press & Schechter (1974, *solid*) and Sheth & Tormen (1999, *dotted*). *Upper panel*: Rescaled halo mass functions are shown with analytic functions. Also we adjust the parameters of the Sheth & Tormen function to fit the simulation results (*dashed line*).

show significant differences from other results especially at high redshifts. This discrepancy is due to the different definitions of halos inherent in the halo-finding methods. Sheth & Tormen (1999) have applied their analytic form to the mass functions obtained by the FoF method, treating a sub-halo not as a halo but as a substructure of its host halo. Therefore, the substructure does not play any role when populating galaxies in a halo when the Sheth & Tormen function is adopted. To distribute galaxies in a FoF group they have to introduce a parametric model, the Halo Occupation Distribution (Zehavi et al. 2005), in which the average number of galaxies are determined by the mass of the host halo (the FoF group) and the distributions of mock galaxies are arranged to fit the two-point correlations of real galaxies. Rather than using such a sophisticated and indirect method, we adopt the one-to-one correspondence model that links a galaxy with the PSB halo assuming that each PSB halo hosts a single galaxy and, if a PSB halo is dissolved by tidal interactions or ram pressure in the host halo, its accompanying galaxy is regarded to be completely destroyed.

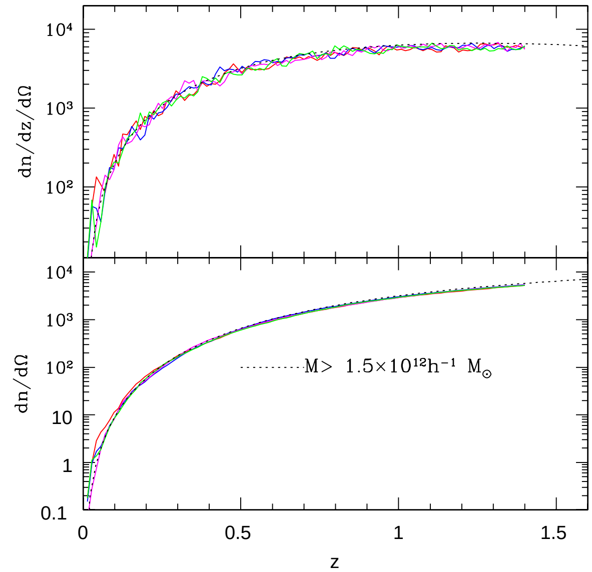

Fig. 2. Halo distributions in the lightcone space seen by four mock observers. *Upper panel*: Shown are halo number densities per unit redshift and solid angle. *Lower panel*: Halo number densities integrated to z are shown. Dotted curves are the analytic functions with modified parameters of the Sheth & Tormen form.

4.2. *Halo Distributions in the Lightcone Space*

To check whether the lightcone data are built properly, we have compared simulation results with analytic predictions of halo distributions. The comoving volume V_c per unit z and solid angle is obtained by (Hogg 1999)

$$\frac{dV_c}{dz d\Omega} = d_H^3 E(z) \left[\int_0^z E(z')dz' \right]^2 , \quad (1)$$

where $d_H \equiv 3000\ h^{-1}$ Mpc and

$$E(z) = 1/\sqrt{\Omega_m(1+z)^3 + \Omega_k(1+z)^2 + \Omega_\Lambda}. \quad (2)$$

Then, the number density of halos $dn(z)/d\Omega dz$ can be obtained as

$$\frac{dn(z)}{d\Omega dz} = \int_{M_{min}}^{\infty} \Phi(M,z) \frac{dV_c}{d\Omega dz} d\log_{10} M, \quad (3)$$

where we set $M_{min} = 1.5 \times 10^{12}\ h^{-1}\ M_\odot$ which is the halo mass resolution ($\sim$ collective mass of 20 particles) of the simulation.

In Figure 2 we show the distribution of halos in the lightcone space. The number density $dn(z)/d\Omega dz$ (*upper panel*) and its cumulative number density $dn(z)/d\Omega$ (*lower panel*) are shown with analytic predictions (*dotted curves*) and four mock

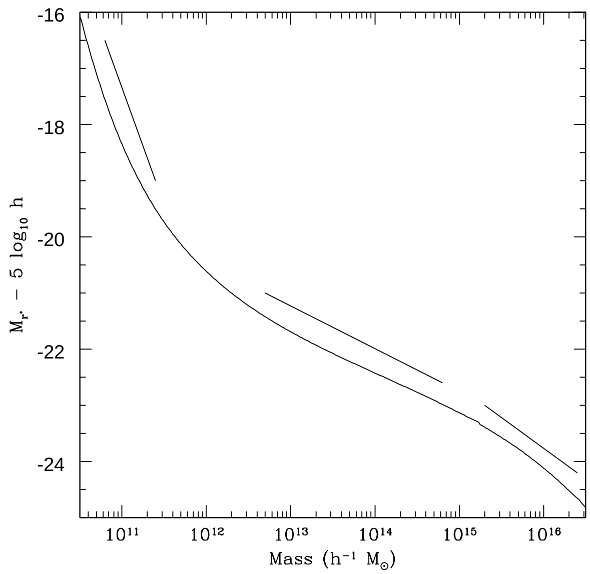

Fig. 3. $\mathcal{M}$–M relation. From upper left, each line segment shows the power-law L–M relation; $L \propto M^{1.67}$, $L \propto M^{0.30}$, and $L \propto M^{0.44}$.

observational results (*solid curves*). There are small variations for different observers but no significant deviation from analytic functions can be seen.

4.3. *Simulating Galaxy*

As briefly depicted above, the mock survey of galaxies is taken by simple assumption of the one-to-one correspondence and the-bigger-the-brighter models. For the latter model, we adopt the r^*-band luminosity function of the SDSS galaxies;

$$\phi(\mathcal{M}) = 0.4 \ln 10 \phi_* 10^{(\alpha+1)\mathcal{M}'} e^{-10^{\mathcal{M}'}}, \qquad (4)$$

where $\mathcal{M}' \equiv -0.4(\mathcal{M} - \mathcal{M}_*)$, $\phi_* = 1.46 \times 10^{-2}$, $\mathcal{M}_* = -20.83$, and $\alpha = -1.2$ (Blanton et al. 2001) and the Sheth and Tormen function, $(\Phi_{ST}(M))$, with modified parameters; $a_c = 0.82$, $p = 0.309$, and $A = 0.348$. By equating the two cumulative number densities,

$$\int_{-\infty}^{\mathcal{M}} \phi(\mathcal{M}') d\mathcal{M}' = \int_{M}^{\infty} \Phi_{ST}(M') d \log_{10} M' \qquad (5)$$

we obtain the mass-to-magnitude relation as shown in Figure 3. In this model we can divide galaxies into three populations depending on their mass: the cluster scales $M \geq 10^{15}$ h^{-1} $\mathrm{M}_\odot$, group scales 2×10^{12} h^{-1} $\mathrm{M}_\odot \leq M \leq 10^{15}$ h^{-1} $\mathrm{M}_\odot$, and galactic and sub-galactic scales $M \leq 2 \times 10^{12}$ h^{-1} $\mathrm{M}_\odot$. We draw power-law relations of mass-to-luminosity

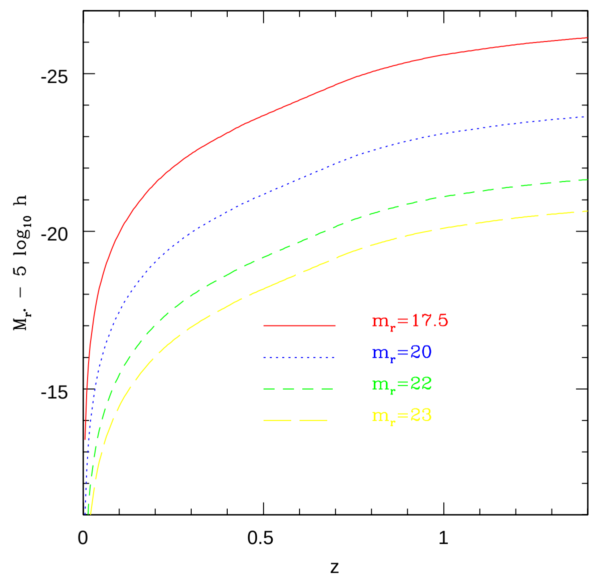

Fig. 4. Relation between absolute magnitude in r^* and redshift for a 6.5-m class telescope.

$(L \propto M^\gamma)$ with $\gamma = 0.44$, 0.30, and 1.67, on high, intermediate, and low mass scales, respectively. We may presume these three phases to stem from different galaxy formation mechanisms and/or different physical quantities of galaxies depending on the halo mass. We will provide the detailed investigations on the $\mathcal{M}$–M relation in a forthcoming paper.

After assigning galaxy luminosities to halos, we calculate their apparent magnitude, correcting for the K and evolutionary effects. We simply use the K correction term, $KC(z)$, and evolutionary correction term, $EC(z)$, derived from the template spectrum of ellipticals by Poggianti (1997). Since the $KC(z)$ has an opposite sign to the $EC(z)$, the net effect of $(K+E)C$ does not grow significantly even at high redshifts. And the difference of $(K+E)C$ between the ellipticals (E) and spirals (Sa) is less than 0.5 at $z \leq 0.5$ and peaks at 1 when $z \sim 1.5$. The observed magnitude, m, of a mock galaxy can be calculated by

$$m = \mathcal{M} + 5 \log \frac{D(z)}{10\mathrm{pc}} + KC(z) + EC(z), \qquad (6)$$

where

$$D(z) = d_H(1+z) \int_0^z E(z')dz'. \qquad (7)$$

Based on these calculations, we measure the number densities of mock galaxies under various magnitude-limits. First, we estimate the required observation time when using a 6.5-m class telescope

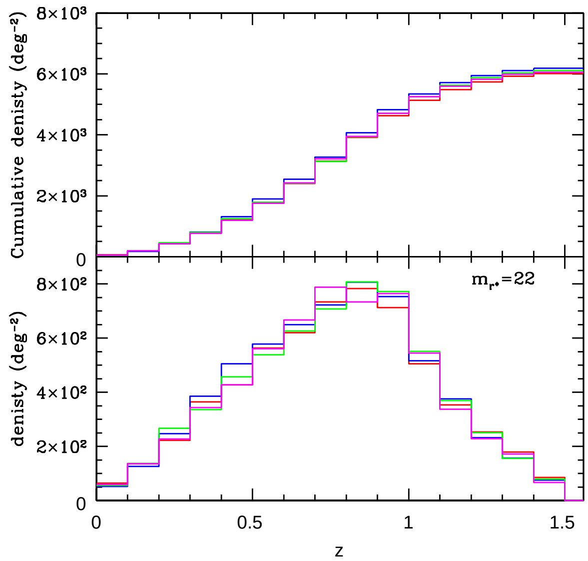

Fig. 5. Histogram of observed galaxies. *Lower panel*: Differential number densities of mock galaxies for four observes are shown if $r^* \leq 22$. *Upper panel*: Cumulative number densities of mock galaxies with the same observational conditions as in the upper panel.

by linearly extrapolating the relation of the Apache Point Observatory telescope size to the exposure time in the SDSS. Since galaxies of apparent magnitude $r = 17.77$ can be spectroscopically observed within 45 minutes by the 2.5-m telescope, we may expect to obtain spectra of galaxies of $r = 22$ by a 6-hour exposure. We are not taking into account the surface brightness dimming effects and the size reduction effects explicitly. Figure 4 shows the $\mathcal{M}_{r^*}$–z relation of several observational magnitude limits. Galaxies of $\mathcal{M}_{r^*} \lesssim -21$ will be completely sampled up to $z = 1.4$ under the observational constraint $r^*_{lim} \simeq 22$. Their distribution histograms in redshift space when $r^* = 22$, obtained by four observers, are shown in Figure 5. The median galaxy distribution peaks at the bin of $z = 0.8$–0.9 with $dn/dzd\Omega \sim 7500$.

4.4. *Galaxy Distributions*

We show part of the projected distribution of galaxies in a mock survey in Figure 6. The faint-end magnitude of the mock survey is set to $r^* = 22$ and the wedge dimensions are $\Delta\theta = 2\,\text{deg}$, $\Delta\phi = 18.18\,\text{deg}$, and $1100 < d < 1700\ h^{-1}$ Mpc which is about 1.6 % of the proposed volume of the HDS. A wealth of structures such as clusters, filaments, and voids are seen in this mock slice. Interestingly, the luminosity bias in the clustering of galaxies is naturally produced; the brighter galaxies show stronger clustering.

5. COMPARISON WITH OTHER PLANNED SURVEYS

In Figure 7 we show the target numbers and survey volumes of various completed and future redshift surveys for comparison. While the proposed survey time of the HDS is four times larger than the KAOS, the total number of observed galaxies in the HDS is only twice as large as the KAOS due to the reduction by half of the light-gathering power of the applied telescope. But KAOS does not sample entire galaxies within the magnitude limit and only $\sim 5\%$ of the targets will be spectroscopically observed. This kind of sparse sampling has an advantage in covering the larger volume and in the study of baryonic oscillation of galaxy clusterings. Besides these, there are many other projects being proposed. The AAOmega[4] is planning to observe 1.5×10^5 galaxies in $0.5 < z < 0.9$ and in $1000\,\text{deg}^2$ solid angle with the 3.9-m telescope of the Anglo-Australian observatory. Also, in China, the LAMOST[5] (Large Sky Area Multi-Object Fiber Spectroscopic Telescope) project is designed to constrain the equation of state of dark energy ω by analyzing the Alcock & Paczynski effect on the correlation function of galaxies. For that purpose, a fiber-fed spectrograph for simultaneous observation of 4000 targets will be applied to build a catalog of 2×10^7 galaxies brighter than 20.5 magnitude using a 4-m telescope.

The only contender of the HDS is the KAOS in that total target number and the survey volumes of the two are similar to each other. Because of the sparse sampling the KAOS is intended to detect the baryonic bump, as a standard ruler, imprinted on the correlation function to measure the geometry of the universe. About nine times more sources will be observed by the LAMOST than the HDS, but relatively brighter galaxies ($m < 20.5$) will be targeted within a smaller distance, $d = 1300\ h^{-1}$ Mpc, which is less than half of the depth of the HDS survey region. Since the HDS has 6–15 times larger survey volume and 8–24 times larger samples than the other surveys, the observational data of the HDS will provide a more useful basic research resource for the study of galaxy formation and evolution.

The total required time of the HDS is about 6000 hours; the project term can span about two years. Unlike the SDSS which had to make photometric and spectroscopic observations from the beginning,

[4]http://www.aao.gov.au/local/www/aaomega/
[5]http://www.lamost.org/

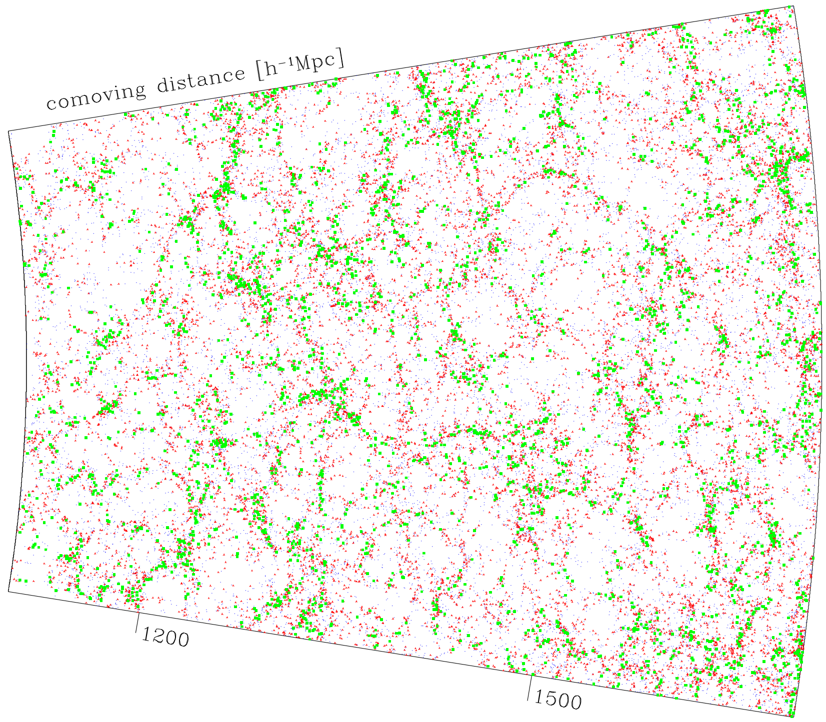

Fig. 6. Simulated galaxies of $r^* < 22$ in the wedge of lightcone space. Three types of symbols represent galaxies in the absolute magnitude ranges as $-21.5 \leq \mathcal{M}_{r^*} \leq -21$ (*dot*), $-22 \leq \mathcal{M}_{r^*} \leq -21.5$ (*skeletal triangle*), and $\mathcal{M}_{r^*} \leq -22$ (*box*).

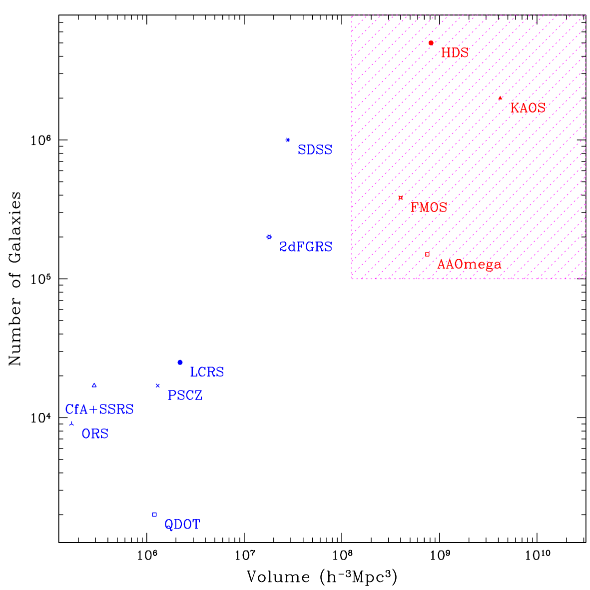

Fig. 7. Survey volumes and target numbers of completed projects and future ones (in the shaded region). The FMOS project is a subproject for observing high–z galaxies in the KAOS.

the HDS may utilize the photometric data already released by other photometric surveys in the 2010's.

6. SCIENTIFIC GOALS

6.1. *Galaxies*

Through the HDS project we will unveil the formation and evolution of the LSS in detail. The spectroscopic data of five million galaxies to one third of the depth of the universe will enable us to study the environmental effect on the galaxy formation and the provenance of the morphological differences (Park & Choi 2005). From this huge galaxy catalog, the variation of galaxy number density in redshifts, two-point correlation function (Park & Lee 1998) on sub-megaparsec scales, power spectrum (Park & Park 2006; Park et al. 1994), luminosity function (Blanton et al. 2001), peculiar velocity field of galaxies, spatial distribution of galaxy groups and clusters, and their redshift dependence could be investigated with high precisions. From the simulation results, we have found two-point correlation function and power spectrum become accurate enough to adopt as theoretical values only if the survey volume is more than $10^9 h^{-3}$ Mpc^3 in order to reduce the noise effect that inherently occurs in small-volume surveys.

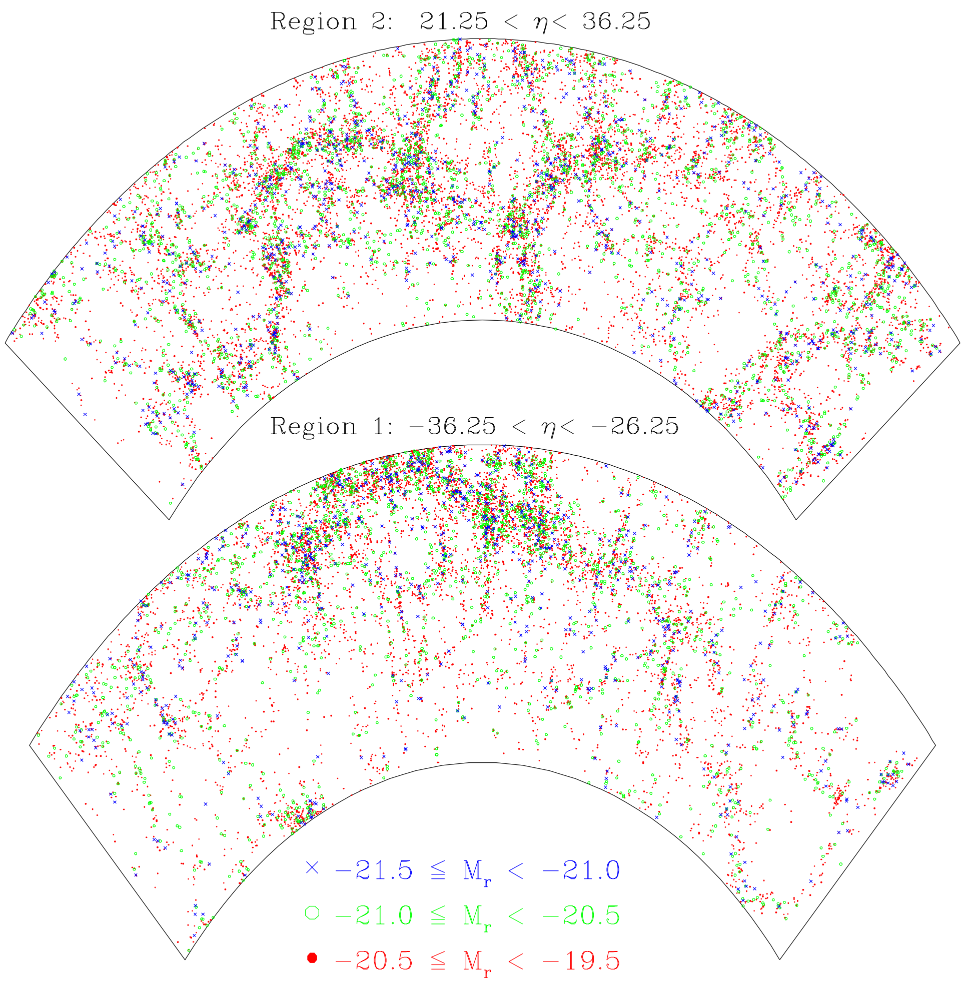

Fig. 8. Galaxy distribution observed by the SDSS. Galaxies in different magnitude ranges are colored in blue, green, and red according to the absolute magnitudes. In the lower panel, the well-known Sloan Great Wall can be easily seen in the upper central part of the region.

Figure 8 shows the biased clustering of the SDSS galaxies in different absolute magnitude ranges. Bright galaxies (*boxes*) show more clustering and faint galaxies (*dots*) are widely spread over the under-dense regions. Also, the CfA2 galaxy redshift survey has shown similar features (Park et al. 1994), which clearly indicate that the galaxy formation mechanism can vary depending on the local environment or density. Since most galaxies have undergone evolution at redshifts less than 1.4, we may study the dependence of biased formation and clustering on the local environment. Since a Luminous Red Galaxy (LRG) as well as Ultra LRG that are supposed to be progenitors of current massive galaxies are included in the research interests of the HDS, we can extend the study of the biased galaxy formation to higher redshifts.

6.2. *Quasars*

Quasars are consequences of gigantic energy eruption by super massive blackholes in the centers of galaxies that are undergoing formation or merging periods. Therefore, the observation of quasars is indirectly related to the galaxy formation study. During the execution of the HDS, we will select quasar candidates from the point-source catalogs based on the photometric properties (Schneider et al. 2005) of known quasars. By follow-up spectroscopic confirmations, one can identify bright quasars at $z \gg 5$. For example, most distant quasars currently observed in the SDSS are in $6 \lesssim z \lesssim 7$, corresponding to one billion years after the Big Bang. The HDS observations will extend the quasar catalog to the edge of the Dark Era when there were rare, light-emitting sources and the hydrogen was not fully ionized. We

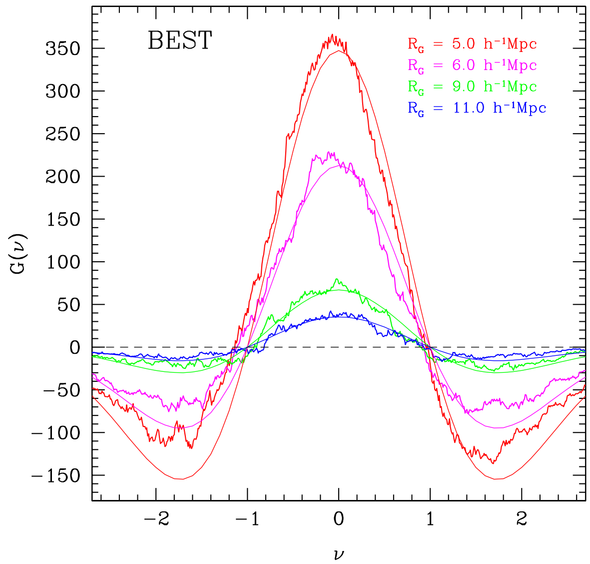

Fig. 9. Genus curve of a sample in the SDSS dr4+ data.

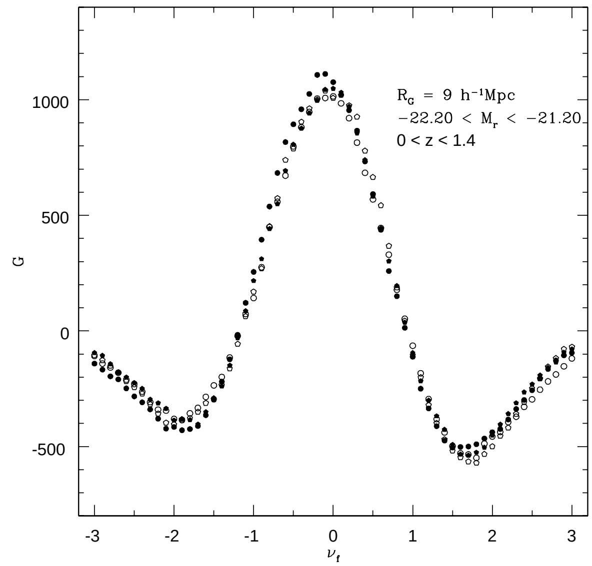

Fig. 10. Genus curve of the simulated galaxies at the smoothing scale of $R_G = 9\ h^{-1}$ Mpc when the mock survey is made within 24% of the HDS in volume. Different symbols are the genus measured by different observers.

want to investigate the quasar luminosity function, evolution of number densities, dependence of galaxy formation activity on the local environments, and clusterings in detail.

6.3. *LSS and Cosmology*

The topology of the LSS provides a useful tool to measure the nonlinearity of cosmic objects. The initial matter fluctuation generated during the inflationary epoch is believed to be Gaussian with random phases. But the gravitational force makes matter fluctuations deviate from the Gaussian and, therefore, higher-order quantities such as three-point correlations and the genus acquire non-Gaussian features.

In Figure 9 we show the genus curves of the density fields built by smoothing the distribution of the SDSS galaxies with four Gaussian smoothing lengths. Even though there are small deviations from Gaussian features in the figure, it shows that galaxy distribution is consistent with Gaussian. Unlike other planned spectroscopic surveys which either sample galaxies sparsely or cover rather small parts of the whole sky, a wide, dense, and deep galaxy sample of the HDS will allow one to measure the higher-order statistics and to reach definitive conclusions on whether a primordial density field is Gaussian, after correcting for the effects of gravitational evolution.

To show how accurately topology can be measured from the HDS data, we measure simulated genus in the four mock surveys. The mock regions are about 24% of the proposed HDS regions in volume. Figure 10 shows the resulting genus curves of a density field produced by smoothing mock galaxies with $R_G = 9\ h^{-1}$ Mpc. There is no significant deviation among different observers, and the same characteristic non-Gaussian features in the statistics, $\Delta\nu$, ΔA_C, and ΔA_V, (for definitions, refer to Park et al. 2005) as in the SDSS observations (Fig. 9) can be seen.

7. DISCUSSION

We propose a next-generation redshift survey that can be made by a 6.5-m aperture telescope. The survey region has a depth $d_H = 3000\ h^{-1}$ Mpc, and a solid angle $\Delta\Omega = 295\,\mathrm{deg}^2$, and includes five million galaxies with magnitudes down to $r^* = 22$ in roughly 250 days of observing time. To achieve this goal, a fiber-fed spectrometer should be designed to observe five thousand objects in a single exposure.

A volume-limited catalog of galaxies up to $z = 1.4$ will provide high-quality statistical precisions to galaxy-related quantities. There are few rival spectroscopic projects. An exception would be the KAOS which will perform sparse sampling over a wider solid angle. The main interest of the KAOS project is to detect the baryonic oscillation effects in the distribution of galaxies dedicating about one year for the observations. The HDS is proposed as an extension of the SDSS which is a wide and dense survey. It will be able to reveal the evolution of the small-scale structures and high-order moments of large-scale structures as its main galaxy sample will reach the high redshifts beyond $z = 1$ unlike the SDSS.

REFERENCES

Abazajian, K., et al. 2003, AJ, 126, 2018

Baldry, I. K., et al. 2002, ApJ, 569, 582

Blanton, E. L., et al. 2001, AJ, 121, 2358

Colless, M. M. 1999, in 14th IAP Coll., Wide Field Surveys in Cosmology, ed. S. Colombi, Y. Mellier & B. Raban (Paris: Editions Frontieres), 77

Dubinski, J., Kim, J., Park, C., & Humble, R. 2004, NewA, 9, 111

Hogg, D. W. 2002, astro-ph/0105280

Hogg, D. W. 1999, astro-ph/9905116

Huchra, J. P., Geller, M. J., de Lapparent, V., & Burg, R. 1988, in IAU Symp. 130, Large Scale Structures of the Universe, ed. J. Audouze, M.-C. Pelletan & S. Szalay (Dordrecht: Kluwer), 105

Kim, J., & Park, C. 2006, ApJ, 639, 600

Loveday, J., Efstathiou, G., Peterson, B. A., & Maddox, S. J. 1992, ApJ, 400, L43

Madau, P., Ferguson, H. C., Dickinson, M. E., Giavalisco, M., Steidel, C. C., & Fruchter, A. 1996, MNRAS, 283, 1388

Neyrink, M. C., Hamilton, A. J. S., & Gnedin, N. Y. 2004, MNRAS, 348, 1

Park, C., & Choi, Y.-Y. 2005, ApJ, 635, L29

Park, C., & Lee, S. 1998, J. Korean Astron. Soc., 31, 105

Park, C.-G., & Park, C. 2006, ApJ, 637, 1

Park, C., Vogelely, M. S., Michael, S., Geller, M. J., & Huchra, J. P. 1994, ApJ, 431, 569

Poggianti, B. M. 1997, A&AS, 122, 399

Press, W. H., & Schechter, P. 1974, ApJ, 187, 425

Ratcliff, A., Shanks, T., Parker, Q. A., & Fong, R. 1998, MNRAS, 293, 197

Schneider, D. C., et al. 2005, AJ, 130, 367

Shectman, S. A., Landay, S. D., Oemler, A., Tucker, D. L., Lin, H., Kirshner, R. P., & Schechter, P. L. 1996, ApJ, 470, 172

Sheth, R. K., & Tormen, G. 1999, MNRAS, 308, 119

Spergel, D. N., et al. 2003, ApJS, 148, 175

Stoughton, C., et al. 2002, AJ, 123, 485

York, D., et al. 2000, AJ, 120, 1579

Zehavi, I., et al. 2005, ApJ, 630, 1

Zucca, E., et al. 1997, A&A, 326, 477